Short-range order in glycerol. A molecular dynamics study

Leslie J. Root[a] and Frank H. Stillinger
AT&T Bell Laboratories, Murray Hill, New Jersey 07974

A molecular model has been constructed for glycerol and has been applied to a study of clusters and condensed phases by molecular dynamics simulation. Each molecule is regarded as a flexible polar complex of nine mass points (CH and CH_2 groups are treated as "united atoms"). Periodic arrays stabilize in a close approximation to the observed glycerol crystal structure, with identical extended molecules connected by infinite chains of hydrogen bonds. By contrast the stable and supercooled liquids display a variety of asymmetrical molecular conformations and an irregular network of hydrogen bonds. Detailed examination of the various atomic pair correlation functions reveals considerable overlap of intramolecular and intermolecular features, implying intrinsic ambiguity in the interpretation of x-ray and neutron diffraction measurements designed to determine the short-range order of liquid glycerol.

I. INTRODUCTION

Glycerol is notorious for its ability to supercool and to vitrify at low temperatures into a rigid glass.[1] These attributes have spawned a wide range of experiments on this substance which have measured virtually all its significant physical properties in stable and metastable phases.[1-5] A correspondingly thorough understanding of structure and dynamics at the molecular level for undercooled glycerol, though presently unavailable, would undoubtedly help to explain the behavior of a broad family of other glass formers.

For reasons related to its glass-forming capacity in pure form, glycerol has technological importance as a cryoprotective agent.[6] It also plays a direct biological role in living organisms, some of which are known to accumulate the substance as part of their cold-hardening process.[7] Glycerol furthermore serves as a convenient liquid medium for various spectroscopic studies of biological molecules.[8,9]

On account of molecular flexibility, asymmetry, and ability to form hydrogen bonds, glycerol is obviously a complex substance. For that reason computer simulation with an acceptable molecular model for glycerol offers considerable advantage for interpreting experiments in detailed molecular terms. This paper reports the development of such a molecular model and its initial exploration using the molecular dynamics method.[10]

Section II defines our dynamical model for glycerol. It is tested in Sec. III to verify that it is consistent with the known stable crystal structure.[11] Section IV considers the dynamics of the free molecule and of small isolated molecular clusters, using the mass-weighted descent mapping to identify isomeric structures and their transitions. Section V reports some calculations for both the stable liquid above the melting point and the strongly supercooled liquid near the measured glass transition temperature range. We conclude this paper with a discussion in Sec. VI of several issues, including the interpretation of neutron and X-ray diffraction measurements.

II. GLYCEROL MODEL

In our view any credible glycerol model to be applied to condensed phase phenomena must include molecular conformational changes, covalent bond deformations, and polarity. This requires a chemically realistic specification of both intramolecular and intermolecular force fields.

Each glycerol molecule contains 14 atoms. We have chosen to exercise one descriptive economy at the outset, namely to treat each of the three carbon atoms and their directly attached hydrogens as single "united atoms" of the appropriate mass. This is justified by the fact that such atom groups do not directly participate in hydrogen bonding. By contrast the three polar hydroxyl groups have been treated as separate oxygen and hydrogen atoms. Thus for present purposes each glycerol molecule is a mechanical system of nine mass points connected by eight covalent bonds. Figure 1 provides an illustration.

Let vector $\mathbf{R}_i$ comprise the 27 coordinates necessary to specify the spatial position of the ith glycerol molecule. We assume that the total potential energy Φ for a collection of N molecules can be written as follows:
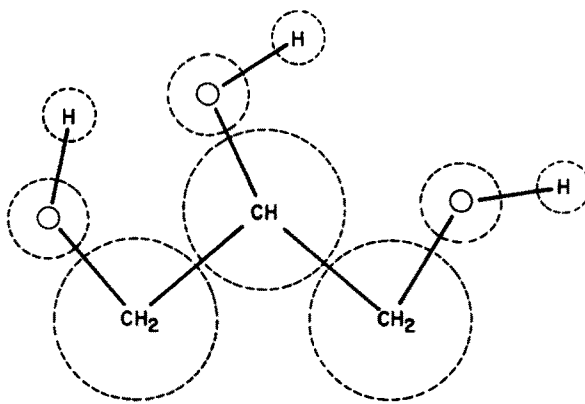

FIG. 1. Molecular model for glycerol. Each carbon atom and its directly attached hydrogens are treated as "united atoms," i.e., single mass points. The O and H electrostatic charges are $\pm 0.34e$.

[a] Present address: Department of Physics, Barnard College, New York, NY 10027.

$$\Phi(\mathbf{R}_1 \cdots \mathbf{R}_N) = \sum_{i=1}^{N} v_1(\mathbf{R}_i) + \sum_{i<j} v_2(\mathbf{R}_i, \mathbf{R}_j). \quad (2.1)$$

Intramolecular interactions are comprised entirely in v_1, while v_2 describes interactions between pairs of molecules. Our model disregards higher-order v_n's, though in principle they should be present.

To develop an explicit potential we sought to achieve a realistic description both of hydrogen bonding and of the internal molecular structure of glycerol. In the absence of disruptive constraints, hydrogen bonds tend to be approximately linear (proton donor, proton, and proton acceptor nearly aligned).[12-14] For oxygen acceptors the hydrogen-bonded O···H distance ranges from about 1.4 to 2.4 Å.[12-14] Hydrogen bond cohesive energies lie in the neighborhood of 5 kcal/mol.[12,13,15] We have ensured that our model displays these features.

Other data taken into consideration as guidance in selecting the model functions v_1 and v_2 are the observed crystal structure of glycerol,[11] molecular structures in the liquid inferred from x-ray[16] and neutron[17,18] scattering, and the results of *ab initio* quantum mechanical calculations for the isolated glycerol molecule.[19,20]

The intramolecular potential function v_1 has been assigned four contributions: covalent bond stretch, covalent bond bend, Coulombic interactions, and Lennard-Jones interactions:

$$v_1(\mathbf{R}) = v_{\text{stretch}}(\mathbf{R}) + v_{\text{bend}}(\mathbf{R}) + v_{\text{Coul}}^{(1)}(\mathbf{R}) + v_{\text{LJ}}^{(1)}(\mathbf{R}). \quad (2.2)$$

The first two of these have strictly harmonic forms:

$$v_{\text{stretch}} = \frac{1}{2} \sum_{\alpha=1}^{8} K_\alpha (b_\alpha - b_\alpha^{(0)})^2, \quad (2.3)$$

$$v_{\text{bend}} = \frac{1}{2} \sum_{\beta=1}^{8} L_\beta (\theta_\beta - \theta_t)^2. \quad (2.4)$$

Here b_α is the length of covalent bond α, and $b_\alpha^{(0)}$ is its equilibrium value. Angles between covalent bonds impinging on an "atom" are denoted by θ_β, and all such angles are assumed to have tetrahedral equilibrium values:

$$\theta_t = \cos^{-1}(-\tfrac{1}{3}). \quad (2.5)$$

Electrostatic charges, $-q$ for oxygens and $+q$ for their attached hydrogens, produce hydroxl group polarity, and $v_{\text{Coul}}^{(1)}$ comprises terms $\pm q^2/r_{ij}$ for the intramolecular interactions between chemically unlinked pairs of these charges; the three carbon-containing united atoms are uncharged in this model. The function $v_{\text{LJ}}^{(1)}$ collects a set of intramolecular Lennard-Jones interactions,

$$4\epsilon_v[(\sigma_v/r_{ij})^{12} - (\sigma_v/r_{ij})^6] \quad (2.6)$$

which operate between all pairs of atoms in the same molecule that are separated by at least two other atoms along a covalent bond path (there are 20 such intramolecular atom pairs).

The intermolecular function v_2 contains two types of interactions:

$$v_2(\mathbf{R}_i, \mathbf{R}_j) = v_{\text{Coul}}^{(2)}(\mathbf{R}_i, \mathbf{R}_j) + v_{\text{LJ}}^{(2)}(\mathbf{R}_i, \mathbf{R}_j). \quad (2.7)$$

The Coulombic portion arises from the same hydroxyl group charges $\pm q$ as before. Lennard-Jones interactions are included for all pairs of atoms with one member in molecule i, and the other in molecule j.

Table I shows the various parameters needed to complete specification of each of the v_1 and v_2 components. Note that the Lennard-Jones parameter σ_v is different for intramolecular CO pairs and for intermolecular CO pairs; otherwise common ϵ_v's and σ_v's are used throughout. The equilibrium bond lengths $b_\alpha^{(0)}$, and the stretch and bend force constants K_α and L_β are those appearing in a potential developed by Melberg and Rasmussen to describe carbohydrates.[21] An initial guess for charges $\pm q$ derived from the permanent dipole moment of methanol produced unrealistically strong hydrogen bonds, so they were reduced in magnitude by about ten percent. Lennard-Jones parameters published by Melberg and Rasmussen,[21] and by Jorgensen and co-workers,[22,23] provided a useful starting point in our search, but in several cases had to be readjusted to our final values to yield acceptable monomer, dimer, and crystal results.

III. CRYSTAL PROPERTIES

Glycerol crystallizes into an orthorhombic structure, with four symmetry-equivalent molecules per unit cell.[11] Unit cell dimensions are

$$a = 7.00 \pm 0.04 \text{ Å},$$
$$b = 9.96 \pm 0.05 \text{ Å}, \quad (3.1)$$
$$c = 6.29 \pm 0.04 \text{ Å}.$$

Positions of all carbon and oxygen atoms have been established, but those of the hydrogens have not.

The enthalpy of melting of glycerol at 18.2 °C is 4.417 kcal/mol.[24] The enthalpy of vaporization, presumably de-

TABLE I. Glycerol potential parameters.[a]

Bond stretch:			
	Bond	K_α	$b_\alpha^{(0)}$
	OH	1070	0.955
	CO	720	1.410
	CC	510	1.509
Bond bend:			
	Triad	L_β	
	COH	80.0	
	CCO	100.0	
	CCC	50.0	
Coulombic:			
	Atom	Charge	
	O	$-0.34e$	
	H	$+0.34e$	
Lennard-Jones			
	Pair	ϵ_v	σ_v
	OH	0.09	1.80
	OO	0.26	2.80
	HH	0.26	2.45
	CH	0.09	2.81
	CC	0.09	4.10
	CO(intra.)	0.26	3.50
	CO(inter.)	0.26	2.72

[a] Distances in angstroms, angles in radians, energies in kcal/mol.

termined at room temperature, is reported to be 18.189 kcal/mol.[25] Neglecting the small possible temperature discrepancy, the sum of these is probably a good estimate for the cohesive energy of the crystal at its melting point:

$$E_{coh} \cong 22.6 \text{ kcal/mol.} \tag{3.2}$$

To obtain the corresponding quantity at absolute zero it is necessary to have crystal and vapor heat capacities from the melting point downward; we are not aware that the latter is available. Probably E_{coh} (0 K) is slightly larger than the melting point estimate (3.2).

Calculations have been carried out to determine if our glycerol model potential is consistent with the observed crystal structure and cohesive energy. An exhaustive search over all reasonable crystal structures was not feasible because of the molecular complexity involved. However, we did examine the orthorhombic case at several alternative densities, with unit cell dimension ratios held fixed, according to Eqs. (3.1). Our starting point was a set of eight unit cells (32 molecules) in an orthorhombic box with dimensions twice those in Eqs. (3.1), $14.00 \times 19.92 \times 12.58$ Å, subject to periodic boundary conditions. The carbon and oxygen atoms were placed at the experimental positions, and the hydrogen atoms were arranged to form linear hydrogen bonds to neighboring molecules (the ony reasonable option in our opinion). Starting points for other densities simply involved homogeneous scaling of all atomic coordinates. Each case was then relaxed to a potential energy minimum, allowing all atoms to displace, by a combination of mass-weighted gradient descent and conjugate gradient techniques. Long-ranged Coulomb interactions were handled by the Ewald summation technique,[26] for which inclusion of the 2196 reciprocal lattice vectors nearest the origin yielded very accurate forces and energies. An Appendix summarizes Ewald summation equations required for orthorhombic symmetry.

Figure 2 shows the potential energies for fully relaxed systems, plotted against the volume reduced by the experimental volume for crystalline glycerol. The lowest potential energy obtained is
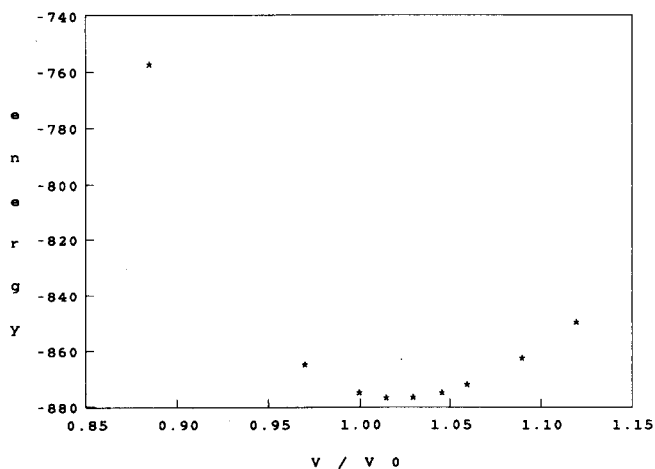
$$\Phi = -876.26 \text{ kcal/mol,} \tag{3.3}$$

corresponding to a system expanded by 0.5% in each direction (this is within the error of experimental determination of the lattice constants).

Conformations and energies of the mechanically stable isomers of the glycerol monomer are discussed in the following Sec. IV. The most stable of these has potential energy equal to -3.2042 kcal/mol. Consequently the absolute-zero cohesive energy of our model crystal is

$$E_{coh} = 876.26/32 - 3.2042$$

$$= 24.18 \text{ kcal/mol.} \tag{3.4}$$

This is reasonably close to the higher-temperature experimental estimate in Eq. (3.2), and as expected a bit larger in magnitude.

Figure 3 presents the most stable model crystal structure, corresponding to the minimum in Fig. 2. Positions of oxygen and carbon atoms are nearly superposable with those seen in experiment. The conformation of each glycerol molecule is "α-α" in the notation Bastiansen,[11,27] not the most stable form apparently for an isolated molecule (see Sec. IV). This α-α conformation favors formation of approximately linear intermolecular hydrogen bonds. We observe that each hydroxyl hydrogen participates in exactly one hydrogen bond, yielding a total of twelve hydrogen bonds per unit cell. The O---H distances in these intermolecular hydrogen bonds range from 1.87 to 2.10 Å; the O–H---O angles range from 139.5° to 161.8°. The hydrogen bonds form infinite chains which globally connect all molecules together. No closed polygons of hydrogen bonds occur in the crystal structure.

IV. CLUSTER PROPERTIES

We next examine a few properties of small clusters of glycerol molecules, including the monomer.

On account of its flexibility, an isolated molecule is capable of exhibiting several alternative isomeric forms. A convenient way to discover, classify, and interconvert these isomers is classical molecular dynamics supplemented with mapping of instantaneous configurations onto potential energy minima. This mapping is generated by solution of mass-weighted gradient descent equations, and was originally devised to investigate inherent structure in liquid and amorphous solid systems.[28–31]

FIG. 2. Potential energy vs volume for the optimized 32-molecule crystal. V_0 is the experimental volume at 1 atm.
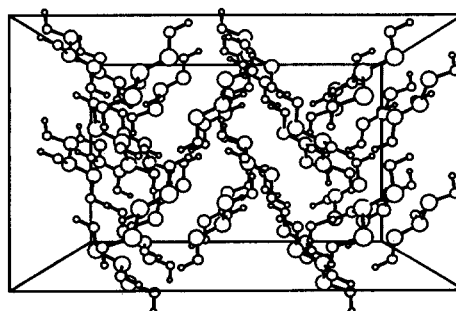

FIG. 3. Optimized crystal structure for the glycerol model. The volume is fixed at the experimental 1 atm value.

Figure 4 shows an example of the mapped potential values (potential minima) obtained during a typical monomer dynamical sequence that lasted 4.9 ps. The conserved total energy of the monomer during this interval was 7.698 16 kcal/mol, and its mean kinetic energy corresponded to a temperature of about 250 K. The dynamics in this case entails visits to potential energy "basins" surrounding four distinct types of minima, i.e., four distinct glycerol isomers.

By varying initial conditions, different portions of the monomer configuration space can be explored. In this way we have discovered 13 distinct glycerol isomers for the monomer in our model. The most stable of these, the absolute potential minimum, lies at − 3.2042 kcal/mol. Its structure is shown in Fig. 5, and can be described as having two severely distorted, and hence weakened, intramolecular hydrogen bonds. This structure is relatively compact and does not resemble the molecular conformation found in the crystal.

An isomer with a more open structure similar to that in the crystal is presented in Fig. 6. Its energy is − 2.0225 kcal/mol. Notice that the three "carbons" and two terminal oxygens are approximately coplanar and form the shape of a flattened "W".

The same dynamical mapping approach has also proved to be a valuable tool for investigation of larger clusters.[32] The most stable form of the glycerol dimer that we have encountered with this approach is displayed in Fig. 7. Two nearly linear intermolecular hydrogen bonds appear, with the same molecule acting as proton donor for both. In addition, each molecule can be described as having a strained intramolecular hydrogen bond. The energy of this dimer is − 20.2088 kcal/mol; subtracting twice the energy of the most stable monomer yields a dimer binding energy of 13.800 kcal/mol.

In consideration of supercooled liquids and amorphous solids, icosahedral groupings of 13 particles have often been given special prominence.[33-35] This arises from the fact that with simple spherical interactions at least, the most stable arrangement of 13 particles is indeed icosahedral with one at the center symmetrically surrounded by the others. The extent to which 13 glycerol molecules might be able to adopt an icosahedral structure consequently becomes a significant question for this well known glass former.

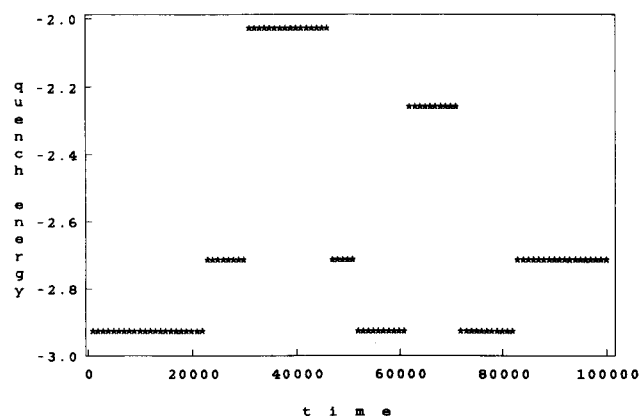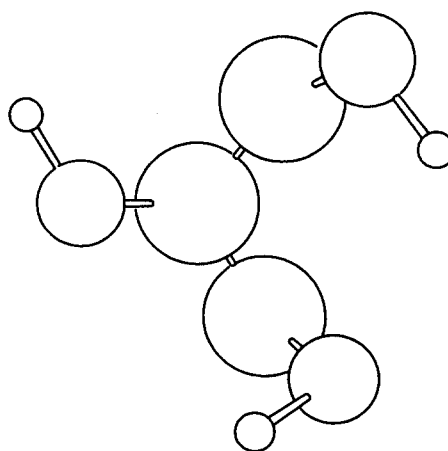To investigate this situation, an initial 13-molecule con-

FIG. 5. Optimized monomer structure.

figuration was created using 12 displaced but otherwise identical replicas of a central molecule in the isomer conformation shown in Fig. 6. The displacement vectors had identical lengths 6.657 Å and pointed to the vertices of a regular icosahedron with edge length 7.000 Å. This initial configuration was then mapped as before onto the relevant potential energy minimum. The resulting cluster structure appears in Fig. 8; its energy is − 246.97 kcal/mol. While the fully relaxed cluster retains compactness of an icosahedral grouping, it has lost all symmetry. Individual molecules have adopted quite distinct conformations, and no two are equivalent. The molecule originally at the center (numbered 13 in our calculation) still remains buried in the final cluster configuration.

Table II provides a measure of the irregularity in the structure of Fig. 8. It gives distances from the central carbon of molecule 13 to the corresponding central carbons of each of the surrounding molecules. Initially these distances were all 6.657 Å. The relaxation (mapping) to the potential energy minimum has caused shrinkage and considerable dispersion of the distances to occur.

Although we have not repeated this kind of 13-molecule cluster calculation with different initial isomer conformations, we strongly suspect similar results would inevitably be obtained. Evidently the asymmetry of the individual molecules eliminates icosahedral local order as an important structural feature in clusters, and by implication in the extended glass phase. Results reported in Sec. V appear to support this conclusion.
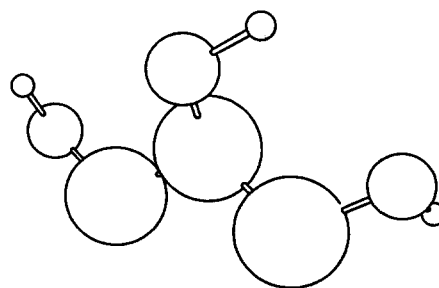

FIG. 6. Monomer isomer with an extended conformation similar to that found in the crystal. This form lies 1.1817 kcal/mol above the globally stable isomer shown in Fig. 5.

FIG. 4. Mapped potential energies for an isolated glycerol molecule with mean kinetic temperature 250 K. The dynamical sequence extends 4.9 ps.
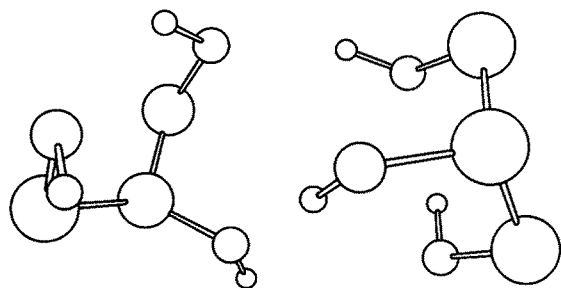
FIG. 7. Glycerol dimer exhibiting a pair of intermolecular hydrogen bonds.

V. LIQUID STRUCTURE

Several sets of molecular dynamics calculations have been carried out to investigate short range order in the liquid phase. The majority of our calculations have involved 32 glycerol molecules (288 mass points) confined to a cubical cell. Periodic boundary conditions were applied to this cell, and consistent with calculations on the crystal (Sec. III) the Ewald summation technique was used to handle long-ranged Coulomb interactions in the infinite periodic array of cells. The fifth-order Gear algorithm[36] was employed to integrate numerically the Newton equations of motion.

The 32-molecule liquid calculations were carried out at fixed volume, with the cubic cell edge equal to 15.073 Å. This corresponds to mass density 1.35 g/cm^3, the observed glycerol glass value extrapolated to absolute zero.[37]

Two temperatures have been studied in detail, 303.2 and 202.4 K. The first corresponds to thermodynamically stable liquid, slightly compressed, just above the melting point. The second corresponds to a strongly supercooled liquid just above the experimental glass transition temperature ($T_g \cong 190$ K). Following a period devoted to internal equilibration, atomic pair correlation functions[38] were evaluated at each of these temperatures as averages accumulated over 20 000 time steps (0.98 ps). At the end of each of these averaging intervals the final system configuration was mapped onto the relevant potential energy minimum to provide static examples of amorphous glycerol glass networks.
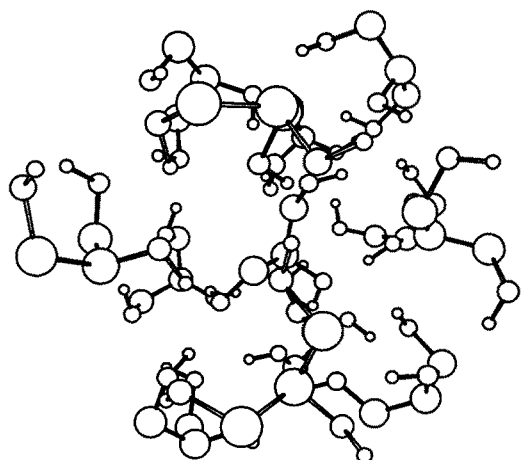
For the evaluation of the pair correlation functions

TABLE II. Distances between central "carbons" in the cluster of Fig. 4, measured from the central molecule to those surrounding it.[a,b]

Molecule	Distance
1	4.466
2	5.793
3	4.962
4	4.355
5	6.015
6	4.564
7	6.532
8	5.392
9	5.689
10	6.271
11	5.946
12	5.676

[a] Distances in angstroms.
[b] Before mapping to the potential minimum all distances were 6.657 Å.

$g_{\mu\nu}(r)$ ($\mu,\nu = $ C,O,H), all 96 carbon atoms were grouped together as a single species, as were all oxygen atoms, and all hydroxyl hydrogen atoms. If the statistics had been more favorable it would have been desirable to distinguish "end atoms" from "center atoms" in each molecule. Because

$$g_{\mu\nu}(r) \equiv g_{\nu\mu}(r) \tag{5.1}$$

there are six distinct functions to be evaluated. These are presented in Figs. 9–14. Each figure contains both high temperature (upper curve) and low temperature (lower curve) results to facilitate comparison. As a general observation, each member of a pair of curves shows the same features as its partner, but the lower temperature case always displays substantially greater distinctiveness (narrower, more intense, better resolved components).

The g_{CC} results in Fig. 9 show a pair of completely resolved peaks at small distance. Both correspond strictly to intramolecular pairs. The shorter distance feature, running off scale at $r \cong 1.5$ Å arises from the 64 directly bonded pairs of carbons. The weaker feature at $r \cong 2.5$ Å arises from the 32 pairs of end carbons in the same molecule, and its greater width reflects primarily the influence of C–C–C bend vibrations. Intermolecular pairs only exist beyond $r \cong 3.5$ Å and yield no sharply defined features at either temperature.

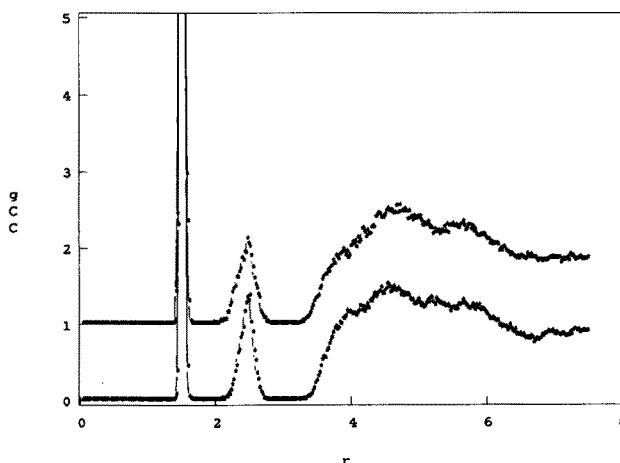FIG. 8. Optimized cluster of 13 glycerol molecules.

FIG. 9. Pair correlation functions for "carbon atoms" in the simulated liquid glycerol. Upper curve, 303.2 K; lower curve 202.4 K.

The closest pairs of oxygens contributing to the g_{OO} functions in Fig. 10 are intramolecular pairs. These are separated by three or four covalent bonds that admit dihedral angle rotations, and so appear correspondingly broadened in their distributions. The larger-distance component, due to pairs of end oxygens, can extend to about 4.8 Å and thus strongly overlaps the intermolecular part of the distribution. Analogous remarks apply to the g_{HH} functions displayed in Fig. 11.

The mixed-species correlation functions g_{CO} shown in Fig. 12 contain three distinguishable intramolecular portions. The shortest and narrowest of these are directly bonded C–O pairs. The next ($r \cong 2.4$ Å) arises from pairs, both of which are covalently bonded to a common intervening carbon, and bond–bend broadening applies. The third (peaking at $r \cong 3.7$ Å) comes from pairs with carbon at one end of a molecule, the oxygen at the other end, and shows substantial broadening due to dihedral angle variation along the intervening C–C–C–O covalent bond chain. The broad maximum at $r \cong 5.0$ Å reflects intermolecular correlation in the liquid.

A small but very significant aspect of the g_{CO} curves in Fig. 12 is the presence of pairs in the range

$$2.6 \text{ Å} \leqslant r \leqslant 3.2 \text{ Å.} \tag{5.2}$$

These are end–end intramolecular pairs with a small intervening dihedral angle. Our investigations (not shown) of the crystal pair correlation functions demonstrate that the range shown in Eq. (5.2) is entirely devoid of CO pairs since all molecules have an extended conformation as illustrated in Fig. 3. Evidently a distribution of molecular conformations characterizes the liquid, with molecules occasionally twisted internally into more compact arrangements than in the crystal.

The isolated peak in g_{CH}, Fig. 13, at $r \cong 2.0$ Å, represents intramolecular pairs covalently bonded to a common oxygen. The larger-distance components involve overlapping intramolecular and intermolecular contributions.

Directly bonded O–H pairs provide the narrow off-scale peaks at $r \cong 1.0$ Å in Fig. 14. Hydrogen-bonded O---H pairs, primarily intermolecular, contribute to the broad feature
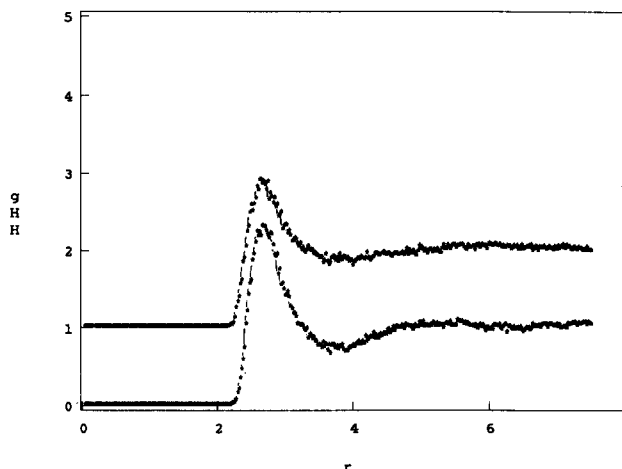

FIG. 11. Pair correlation functions for hydroxyl hydrogens. Upper curve, 303.2 K; lower curve 202.4 K.

peaked at $r \cong 2.0$ Å. The subsequent broad feature at $r \cong 3.5$ Å reveals the presence of pairs more remotely connected along a chain of hyrogen bonds, and shows up quite strongly in the g_{OH} for the low temperature crystal.

The amorphous molecular packings that were obtained by mapping final liquid-run configurations to potential energy minima appear in Figs. 15 and 16. These structures are likely typical of those that would almost always be found by mapping other liquid configurations onto potential minima. Consequently, they can be taken as representative of the "inherent structure" in liquid glycerol.[28–31,39] Careful examination of Figs. 15 and 16, and comparison with the earlier crystal Fig. 3, indeed establishes that the molecular conformations contributing to the liquid phase inherent structure are quite variable, and frequently differ considerably from the crystal counterparts. Intramolecular CO pairs previously found in the range given in Eq. (5.2) for the liquid states persist under mapping, and continue to appear in the structures at the potential energy minima.

Table III contains the potential energy values for the amorphous packings of Figs. 15 and 16. These are less negative than the crystal value obtained earlier, Eq. (3.3). In fact
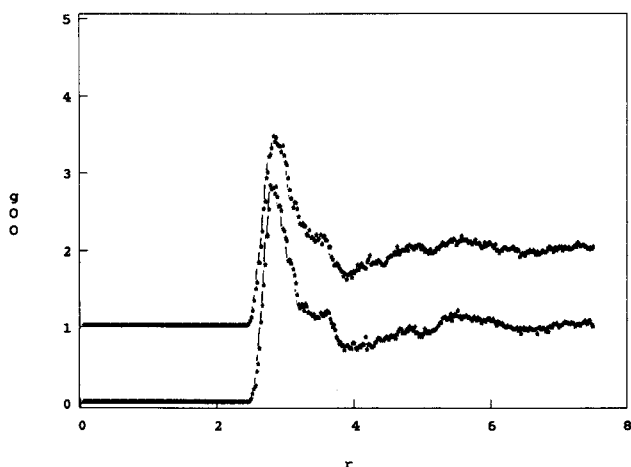

FIG. 10. Pair correlation functions for oxygen atoms. Upper curve, 303.2 K; lower curve 202.4 K.
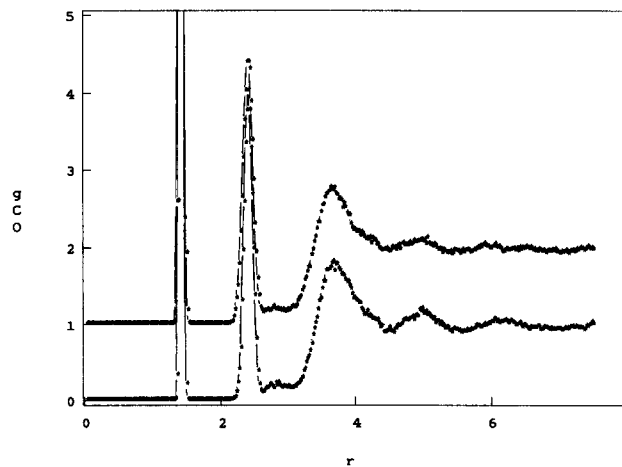

FIG. 12. Pair correlation functions for "carbon"–oxygen pairs. Upper curve, 303.2 K; lower curve, 202.4 K.
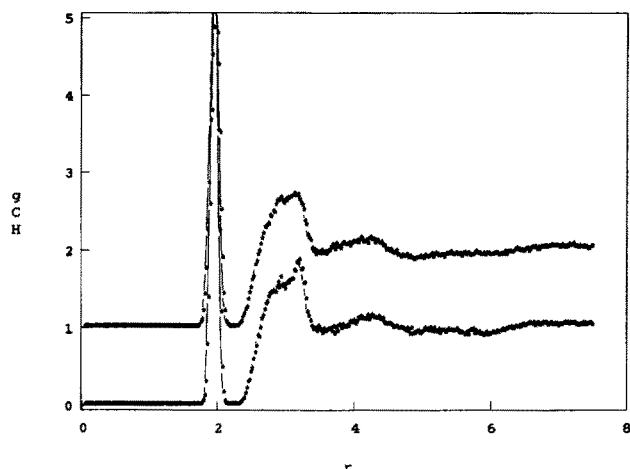
FIG. 13. Pair correlation functions for "carbon"–hydroxyl hydrogen pairs. Upper curve, 303.2 K; lower curve 202.4 K.

FIG. 15. Amorphous molecular packing obtained from the 202.4 K liquid by mass-weighted gradient descent on the multidimensional potential energy surface.

the separation between average amorphous structure potential energy and crystal potential energy may be somewhat larger than the two entries in Table III suggest, since for our model the constrained crystal optimization surely has not quite found the globally stable crystal form.

Table III also contains some hydrogen-bond counts for the two amorphous packings. We have postulated that all OH pairs that are not covalently bonded but that satisfy the distance criterion

$$r_{ij} \leqslant 2.40 \text{ Å} \tag{5.3}$$

are to be regarded as hydrogen bonded. Application of this definition to the crystal structure shown in Fig. 3 identifies the previously mentioned chains of intermolecular hydrogen bonds that involve all hydroxyl groups and *only* these hydrogen bonds are so identified.

The hydrogen bond entries in Table III are distinctly "noncrystalline" in several important ways. First, intramolecular hydrogen bonds appear in these amorphous structures, whereas the crystal contains none. Second, the total number of hydrogen bonds in both cases exceeds that in the crystal (3 per molecule, 96 for the 32 molecules). The in-
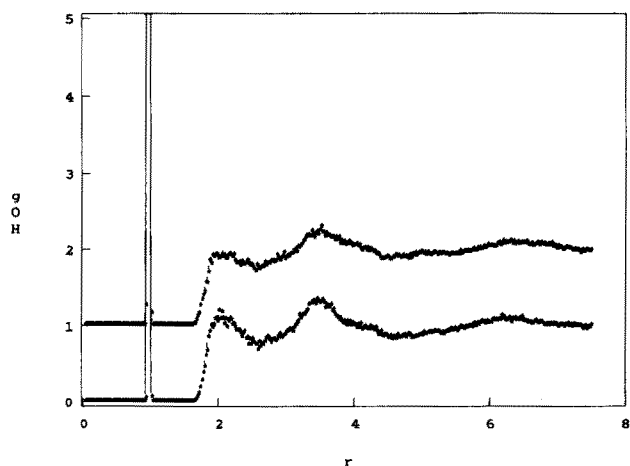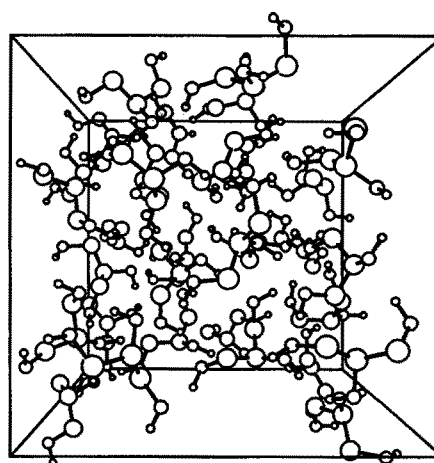
crease in total number of bonds necessarily involves branching in the hydrogen bond network owing to the presence of bifurcated and trifurcated H's and O's. Third, there are some occurrences of missing, or broken, hydrogen bonds. Although we have not attempted to enumerate them in the amorphous packings, one also expects occasionally to find closed rings of intact hydrogen bonds, in distinction to the crystal.

Although all of the results reported in this Section V have involved 32-molecule molecular dynamics calculations, we have also carried out some (necessarily brief) runs on systems of 256 molecules (2304 mass points). The limited data so obtained did not indicate the presence of serious errors in the 32-molecule simulations due to small system size. Nevertheless, it is obviously desirable in the future to utilize larger numbers of molecules in glycerol simulations.

VI. DISCUSSION

As noted earlier both x-ray[16] and neutron[17,18] scattering measurements have been performed on liquid glycerol. The former involved samples at 250 and 350 K, the latter had samples at 193, 293, and 296 K, so that both normal liquid and deeply supercooled states were examined. Tentative conclusions have been drawn in these studies about molecu-

FIG. 14. Pair correlation functions for oxygen–hydroxyl hydrogen pairs. Upper curve, 303.2 K; lower curve, 202.4 K.
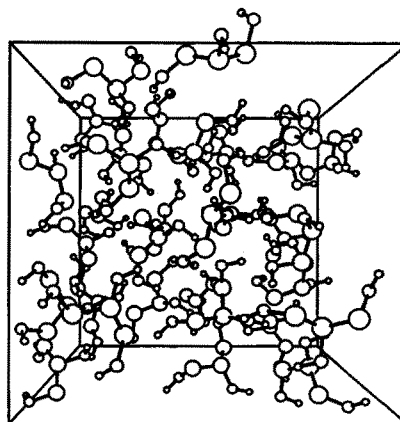

FIG. 16. Amorphous molecular packing obtained from the 303.2 K liquid.

TABLE III. Properties of the amorphous glycerol packings obtained by mapping from liquid state to potential minima.

	Case 1	Case 2
Liquid temperature (K)	202.4	303.2
Figure number	15	16
Packing potential (kcal/mol)	− 872.763 36	− 866.817 57
Total H bonds[a]	108	104
Intermol. H bonds	103	99
Intramol. H bonds	5	5
Bifurcated H bonds[b]	17	11
Trifurcated H bonds[b]	1	1

[a] Defined by distance criterion $r_{ij} \leqslant 2.40$ Å.

[b] Birfurcated and trifurcated H bonds refer to H's simultaneously bonded to two or to three O's, respectively.

lar conformations and about short-range intermolecular order.

While our glycerol modeling may deserve improvement in several respects, it does serve to illustrate the intrinsic difficulties encountered in the interpretation of scattering experiments. It is clear from pair correlation functions shown in Figs. 9–14 that intramolecular and intermolecular atom pairs are not cleanly separated in distance but can overlap substantially. The pair correlation functions $g_{OO}(r)$, Fig. 10, illustrate this most vividly. But this overlap creates an ambiguity of interpretation that is fundamentally insurmountable unless additional information from some other source can be supplied. For this reason, the single elongated molecular conformation observed in the crystal was assumed in the x-ray study of Ref. 16 to persist in the liquid. While neutron scattering Refs. 17 and 18 assumed a more general molecular conformational option, only a single "average conformation" was selected, though in principle molecule–pair conformation fluctuations can exist and would influence scattering. Study of structures such as those shown in Figs. 15 and 16 seem to suggest that this kind of coupling of intramolecular order and intermolecular order is important in glycerol.

Measured temperature dependence of order in glycerol, over the wide temperature ranges that have been considered, is surprisingly small. By contrast, the changes shown in Figs. 9–14 for a comparable temperature range (≈ 100 K) appear to be rather larger. We suspect that the discrepancy may be partly due to cancellations involved in the specific linear combinations of atomic pair correlation functions determined, respectively, by x ray and by neutron experiments. Furthermore, such cancellations may hide real temperature effects on intramolecular conformational ditributions which we have just argued have been imperfectly isolated from intermolecular effects.

The present modeling project should be regarded primarily as a pilot study. More extensive molecular dynamics simulations for glycerol are surely warranted. First, larger systems need to be examined, perhaps containing as many as 10^3 molecules. This would help to assess the experimental observations of weak but definite intermolecular order to about 20 Å[17,18] which the present small-system simulations cannot be expected to reproduce. Second, sufficient statisti-

cal data should be created to provide accurate conformational distributions for the molecules at distinct temperatures. Third, the energy distribution of relative potential energy minima (mechanically stable molecular packings) in the glass-forming substance should be determined by carrying out a large number of descent mappings, to see if the results differ qualitatively from those obtained for simple atomic substance models.[40,41] Fourth, translational diffusion and rotational relaxation rates should be determined and compared with corresponding measurements on the real substance, particularly in the supercooled regime. These studies would be valuable background for subsequent simulations designed to explain the role of glycerol in, e.g., low-temperature hole-burning experiments.[42]

APPENDIX

Hansen[26] has written an excellent discussion of the Ewald summation technique. Here we merely provide the correct expressions for the reader's convenience, and note the modification required to treat an orthorhombic box, rather than the usual cubic case.

The Coulomb part of the potential energy, in general, is given by

$$\Phi_{\text{Coul}} = \frac{1}{2} \sum_i \sum_{j \neq i} \frac{q_i q_j}{r_{ij}}, \tag{A1}$$

where q_i is the charge on atom i and r_{ij} is the distance between atoms i and j. With periodic boundary conditions, the i sum in Eq. (A1) covers all atoms in the primary box, while j covers all atoms aside from i in the primary box as well as all atom images in other boxes (including those of i).

In three dimensions Eq. (A1) can be rewritten[26]

$$\Phi_{\text{Coul}} = \sum_{i<j} q_i q_j \frac{\text{erfc}(\alpha r_{ij})}{r_{ij}} + \frac{2\pi}{V} \sum_{\mathbf{G} \neq 0} \frac{\exp(-G^2/4\alpha^2)}{G^2}$$

$$\times \left\{ \left[\sum_i q_i \cos(\mathbf{G} \cdot \mathbf{r}_i) \right]^2 + \left[\sum_i q_i \sin(\mathbf{G} \cdot \mathbf{r}_i) \right]^2 \right\}$$

$$- \frac{\alpha}{\pi^{1/2}} \sum_i q_i^2. \tag{A2}$$

Here V is the volume of the primary box (the simulation cell) and erfc as usual denotes the complementary error function. All sums now cover only the charges in the primary box, and r_{ij} is to be calculated by the nearest-image convention. For an orthorhombic box with dimensions l_x, l_y, l_z the reciprocal lattice vectors $\mathbf{G}$ are given by

$$\mathbf{G} = (2\pi m_x/l_x)\mathbf{u}_x + (2\pi m_y/l_y)\mathbf{u}_y + (2\pi m_z/l_z)\mathbf{u}_z,$$

$$m_x, m_y, m_z = 0, \pm 1, \pm 2, \ldots, \tag{A3}$$

where $\mathbf{u}_x$, $\mathbf{u}_y$, and $\mathbf{u}_z$ are unit vectors in the x, y, and z directions, respectively. In practice the reciprocal lattice vector sum in Eq. (A2) must be truncated, with $|m_x|$, $|m_y|$, and $|m_z|$ ranging from zero to some appropriate integer n. The parameter α is chosen to produce rapid convergence of the sums. When α and n are correctly selected, Φ_{Coul} remains substantially constant as α is varied over a limited range or as n is increased.

Differentiation of Eq. (A2) is required in order to calculate forces:

$$-\frac{\partial \Phi_{\text{Coul}}}{\partial x_i}$$

$$= q_i \sum_{j \neq i} q_j \frac{(x_i - x_j)}{r_{ij}^2}$$

$$\times \left\{ \frac{\text{erfc}(\alpha r_{ij})}{r_{ij}} + \frac{2\alpha}{\pi^{1/2}} \exp\left[-(\alpha r_{ij})^2\right] \right\}$$

$$+ \frac{4\pi q_i}{V} \sum_{G \neq 0} \frac{\exp(-G^2/4\alpha^2)}{G^2} G_x \left[\sin(\mathbf{G}\cdot\mathbf{r}_i)\right.$$

$$\left. \times \sum_j q_j \cos(\mathbf{G}\cdot\mathbf{r}_j) - \cos(\mathbf{G}\cdot\mathbf{r}_i) \sum_j q_j \sin(\mathbf{G}\cdot\mathbf{r}_j) \right]$$

(A4)

with analogous expressions for the other force components. Lantelme et al.[43] point out that accurate evaluation of the forces requires inclusion of more reciprocal lattice vectors than does correspondingly accurate evaluation of the energy. In our glycerol work we have taken $n = 5$ or 6, so that 1330 or 2196 reciprocal lattice vectors were included. The error in the energy due to truncation of the sum over reciprocal lattice vectors was then of order 1 part in 10^5.

Finally we note that Eqs. (A2) and (A4) differ somewhat from the expressions given by Hansen[26] and by Lantelme et al.[43] We have rewritten the sums over reciprocal lattice vectors so that the computation time for that term increases only linearly with the number of charges,[26] and have also corrected their typographical errors.

[1] A. R. Ubbelohde, The Molten State of Matter (Wiley, New York, 1978), Chap. 16.

[2] D. W. Davidson and R. H. Cole, J. Chem. Phys. 18, 1417 (1950).

[3] R. Piccirelli and T. A. Litovitz, J. Acoust. Soc. Am. 29, 1009 (1957).

[4] C. Demoulin, C. J. Montrose, and N. Ostrowsky, Phys. Rev. A 9, 1740 (1974).

[5] Y. H. Jeong, S. R. Nagel, and S. Bhattacharya, Phys. Rev. A 34, 602 (1986).

[6] C. Polge, A. V. Smith, and A. S. Parkes, Nature 164, 666 (1949).

[7] R. E. Lee, Jr., C.-P. Chen, and D. L. Denlinger, Science 238, 1415 (1987).

[8] D. J. Surman and J. C. Vickerman, J. Chem. Soc. Chem. Commun. 1981, 324.

[9] M. Barber, R. S. Bordoli, R. D. Sedgewick, and A. N. Tyler, J. Chem. Soc. Chem. Commun. 1981, 325.

[10] Molecular-Dynamics Simulation of Statistical–Mechanical Systems, edited by G. Ciccotti and W. G. Hoover (North-Holland, Amsterdam, 1986).

[11] H. van Koningsveld, Rec. Trav. Chim. 87, 243 (1968).

[12] G. C. Pimentel and A. L. McClellan, The Hydrogen Bond (W. H. Freeman, San Francisco, 1960).

[13] S. N. Vinogradov and R. H. Linnell, Hydrogen Bonding (Van Nostrand Reinhold, New York, 1971).

[14] I. Olovsson and P.-G. Jönsson, in The Hydrogen Bond. II. Structure and Spectroscopy, edited by P. Schuster, G. Zundel, and C. Sandorfy (North-Holland, Amsterdam, 1976), pp. 403–408.

[15] P. Schuster, in The Hydrogen Bond. I. Theory, edited by P. Schuster, G. Zundel, and C. Sandorfy (North-Holland, Amsterdam, 1976), pp. 25–163.

[16] M. Soltwisch and B. Steffen, Z. Naturforsch. Teil A 36, 1045 (1981).

[17] D. C. Champeney, R. N. Joarder, and J. C. Dore, Mol. Phys. 58, 337 (1986).

[18] M. Garawi, J. C. Dore, and D. C. Champeney, Mol. Phys. 62, 475 (1987).

[19] L. van den Enden, C. van Alsenoy, J. N. Scarsdale, and L. Schäfer, J. Mol. Struct. 104, 471 (1983).

[20] C. van Alsenoy, V. J. Klimkowski, J. D. Ewbank, and L. Schäfer, J. Mol. Struct. 121, 153 (1985).

[21] S. Melberg and K. Rasmussen, J. Mol. Struct. 57, 215 (1979).

[22] W. L. Jorgensen, J. D. Madura, and C. J. Swenson, J. Am. Chem. Soc. 106, 6638 (1984).

[23] W. L. Jorgensen, J. Phys. Chem. 90, 1276 (1986).

[24] Handbook of Chemistry and Physics, 57th ed., edited by R. C. Weast (Chemical Rubber, Cleveland, 1976), p. C-723.

[25] Reference 24, p. C-735.

[26] Reference 10, pp. 94–99.

[27] O. Bastiansen, Acta Chem. Scand 3, 415 (1949).

[28] F. H. Stillinger and T. A. Weber, Phys. Rev. A 28, 2408 (1983).

[29] T. A. Weber and F. H. Stillinger, Phys. Rev. B 32, 5402 (1985).

[30] F. H. Stillinger and R. A. LaViolette, J. Chem. Phys. 83, 6413 (1985).

[31] F. H. Stillinger and T. A. Weber, J. Chem. Phys. 88, 5123 (1988).

[32] T. L. Beck and R. S. Berry, J. Chem. Phys. 88, 3910 (1988).

[33] F. C. Frank, Proc. R. Soc. London Ser. A 215, 43 (1952).

[34] J. F. Sadoc, J. Non-Cryst. Solids 44, 1 (1981).

[35] P. J. Steinhardt, D. R. Nelson, and M. Ronchetti, Phys. Rev. B 28, 784 (1983).

[36] Reference 10, pp. 52–55.

[37] Reference 1, p. 420.

[38] T. L. Hill, Statistical Mechanics (McGraw–Hill, New York, 1956), Chap. 6.

[39] F. H. Stillinger and T. A. Weber, Science 225, 983 (1984).

[40] T. A. Weber and F. H. Stillinger, J. Chem. Phys. 80, 2742 (1984).

[41] T. A. Weber and F. H. Stillinger, J. Chem. Phys. 81, 5089 (1984).

[42] M. Berg, C. A. Walsh, L. R. Narasimhan, K. A. Littau, and M. D. Fayer, J. Chem. Phys. 88, 1564 (1988).

[43] F. Lantelme, P. Turq, B. Quentrec, and J. W. E. Lewis, Mol. Phys. 28, 1537 (1974).